Kinematic Cusps: Determining the Missing Particle Mass at the LHC

Tao Han[1], Ian-Woo Kim[1], and Jeonghyeon Song[1,2]
[1]*Department of Physics, University of Wisconsin, Madison, WI 53706, USA and*
[2]*Division of Quantum Phases & Devices, School of Physics, KonKuk University, Seoul 143-701, Korea*
(Dated: July 6, 2009)

Neutral massive stable particles (dark matter candidates) are produced at colliders in pairs, due to an exact symmetry called a "parity". They escape from detection, rendering their mass measurement difficult. We consider the pair production of these stable particles associated with two observable particles, from a two-step cascade decay of a heavier particle with even parity, via an intermediate particle with odd parity. We observe kinematic cusp structures in the invariant mass and angular distributions of the observable particles. Knowing the parent mass from direct resonant decay into Standard Model particles, one can determine the missing particle mass as well as the intermediate particle mass by using the cusped peak and end point of the distributions. The shape of the cusp distribution does not depend on the spin correlation.

PACS numbers: 11.80.Cr, 12.60.-i, 14.80.-j

Introduction. Pauli's postulation of a new particle that escapes from detection and carries away energy and angular momentum in β decay not only laid out the foundation for the weak interaction, but also rightfully introduced the first dark matter (DM) particle, the neutrino. Ever since then, attempts to determine the masses and other properties of the neutrinos have led to many research efforts in nuclear physics, particle physics, astroparticle physics and cosmology. If the upcoming experiments at the CERN LHC find evidence of large missing energy events beyond the Standard Model (SM) expectations, it will be a new exciting discovery. Most significantly, this may hold the key to explain the missing mass puzzle in the Universe, the dark matter. It is thus of fundamental importance to determine the mass and properties of this missing particle in LHC experiments, to uncover its underlying dynamics and to check its consistency with dark matter expectations.

However, this task appears to be extremely difficult, even with the establishment of missing energy events at the LHC. In hadronic collisions, the undetermined longitudinal boost of the parton-level scattering leads to the ambiguity of their partonic c.m. energy in the lab frame. Furthermore, with a conserved discrete quantum number (generically called a "parity") that keeps the lightest particle in the new sector stable, the missing particles always come in pairs and thus the final state kinematics is even less constrained. Great efforts have been made to reconstruct the mass of the missing particle in SUSY-like cascade decays. The mass difference of two parity-odd particles may be measured by the maximum end-points of invariant mass distributions [1]. Attempts have been made to determine the missing particle mass by the construction of new transverse variables [2, 3]. With long cascade decay chains, it may be possible to determine the masses through the on-shell mass constraints combining information from multiple events [4].

We propose a more favorable configuration in which the two missing parity-odd particles (X) come along with two visible SM particles (a), from the decay of a heavier parity-even particle (D) through intermediate parity-odd particles (B), as shown in Fig. 1. We dub this decay topology as the "antler" diagram. The advantage of antler decays is that once the parent mass (m_D) is known, the masses of the missing particle (m_X) and the intermediate particle (m_B) can be determined by measuring the energy-momenta of the visible particles (a) without combinatoric complications.

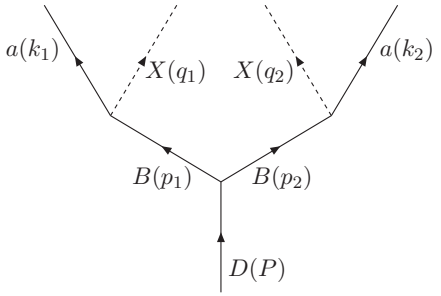

FIG. 1: The "antler" decay diagram, a heavy particle (D) to two visible SM particles (a) and two missing particles (X), via two on-shell intermediate particles (B).

The antler topology is common in many scenarios with DM particle candidates. Familiar examples include the following theoretically well-motivated models:

$$\begin{aligned}
\text{MSSM [5]}, &\quad H \to \tilde{\chi}_2^0 + \tilde{\chi}_2^0 \to Z\tilde{\chi}_1^0 + Z\tilde{\chi}_1^0; \\
Z' \text{ SUSY [6]}, &\quad Z' \to \tilde{\ell}^- + \tilde{\ell}^+ \to \ell^-\tilde{\chi}_1^0 + \ell^+\tilde{\chi}_1^0; \\
\text{UED [7]}, &\quad Z^{(2)} \to L^{(1)} + L^{(1)} \to \ell^-\gamma^{(1)} + \ell^+\gamma^{(1)}; \\
\text{LHT [8]}, &\quad H \to t_- + t_- \to tA_H + tA_H.
\end{aligned} \tag{1}$$

The precondition is that the mass of particle D is known a priori. This can be achieved since its even-parity allows its decay into two observable SM particles. In this regard, the antler topology is equally applicable to a lepton collider where the c.m. energy is accurately known.

Here, we explore two kinematic distributions: (*i*) M_{aa}, the invariant mass of the two visible particles a_1 and a_2, and (*ii*) $\cos\Theta$, cosine of the angle between one of the two

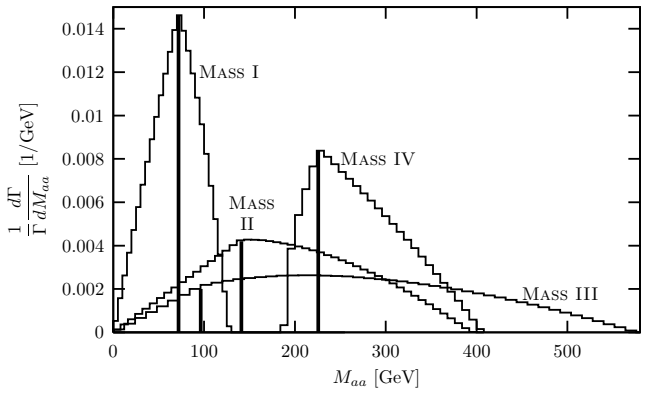

FIG. 2: Normalized differential decay rates versus the invariant mass M_{aa} for various combinations of masses as given in Table I. The vertical lines indicate the positions of the cusps in each M_{aa} distribution.

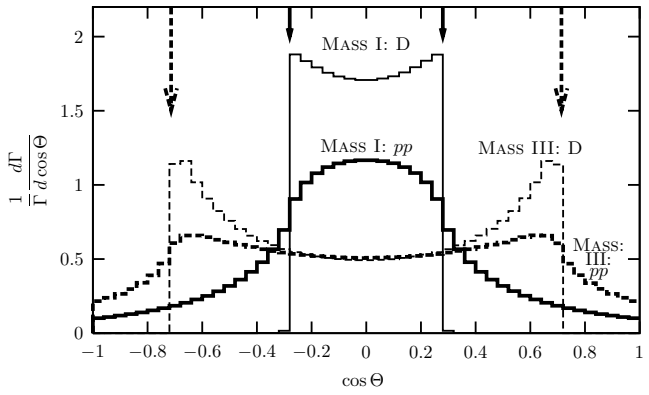

FIG. 3: Normalized differential decay rates versus $\cos\Theta$ in the D-rest frame (thin curves) and in the pp lab frame with $\sqrt{s} = 14$ TeV (thick curves). The parameters of MASS I and MASS III are given in Table I.

visible particles (say a_1) and the pair c.m. moving direction in their c.m. frame. We show these distributions in Figs. 2 and 3. The distributions have, in addition to the end points, unique geometrical structures, the *cusps* (denoted by vertical lines), which carry direct information on m_B and m_X.

A cusp is the point where two curves with different slopes meet. Cusps in the antler decay have outstanding merits for determining the missing particle mass: (*i*) a cusp is experimentally easy to identify due to its pointed feature; its sharpness depends on the mass spectra of the particles involved; (*ii*) looking for a cusp is statistically advantageous since it has large (in most cases, maximum) event rate; (*iii*) cusps can determine both the masses of the intermediate particle B and the missing particle X; (*iv*) there is no combinatoric complication due to its simple decay topology; (*v*) spin correlations of the decay processes do not change the position of the cusps.

The peak features of the cusps arise from the different origins for the M_{aa} and $\cos\Theta$ distributions. Roughly speaking, the triangular shape of the M_{aa} distribution comes from folding diagonally the flat distribution of $d^2\Gamma/d\cos\theta_1 d\cos\theta_2$, where θ_1 and θ_2 are the scattering angles of two visible particles. Reorganized along M_{aa}, the two apexes of the triangle at both ends correspond to $M_{aa}^{\rm min}$ and $M_{aa}^{\rm max}$, while the middle apex corresponds to the cusp. The largest overlapping area below the middle apex explains the largest phase space density. In the distribution about $\cos\Theta$, the on-shell mass condition allows only a limited range for $\cos\Theta$. Since the Jacobean factor leads to a steep increase at the end points, we have a cusp feature in the $\cos\Theta$ distribution. We will leave the details to a future work [9].

Cusp and Edge in M_{aa} Distribution. We first only show the phase space distributions for on-shell particles. It is convenient to use the rapidities: the rapidity η of particle B and the rapidity ζ of particle a in the rest frames of their parents D and B, respectively. In terms of the mass parameters, the rapidities η and ζ are given by

$$\cosh\eta = \frac{m_D}{2m_B} \equiv c_\eta, \quad \cosh\zeta = \frac{m_B^2 - m_X^2 + m_a^2}{2m_a m_B} \equiv c_\zeta.$$

Here and henceforth we use a shorthanded notation of $c_x \equiv \cosh x$. Obtaining the rapidities would be equivalent to measuring the masses m_B and m_X.

(1) $m_a = 0$ case: Consider a to be massless first for simplicity. One would naively expect the invariant mass to have an end-point $M_{aa}^{\rm max} = m_D - 2m_X$. However, due to the on-shell constraint for the particle B, we find a different end-point:

$$M_{aa}^{\rm max} = m_B \left(1 - \frac{m_X^2}{m_B^2}\right) e^{\eta}\,. \tag{2}$$

In addition, the M_{aa} distribution has a cusp at

$$M_{aa}^{\rm cusp} = m_B \left(1 - \frac{m_X^2}{m_B^2}\right) e^{-\eta}. \tag{3}$$

This is remarkable since the ratio $M_{aa}^{\rm max}/M_{aa}^{\rm cusp} = e^{2\eta}$ is governed by the initial decay $D \to BB$ and thus gives m_B. The product $M_{aa}^{\rm max} M_{aa}^{\rm cusp}$ depends on the secondary decay $B \to aX$ and gives m_X. Furthermore, $d\Gamma/dM_{aa}$ is of the form

$$\frac{d\Gamma}{dM_{aa}} \propto \begin{cases} 2\eta M_{aa}, & \text{if } 0 \le M_{aa} \le M_{aa}^{\rm cusp}; \\ M_{aa} \ln\dfrac{M_{aa}^{\rm max}}{M_{aa}}, & \text{if } M_{aa}^{\rm cusp} \le M_{aa} \le M_{aa}^{\rm max}. \end{cases} \tag{4}$$

Figure 2 shows $d\Gamma/dM_{aa}$ for four sets of representative masses specified in Table I. The choice of the parameters for MASS I is motivated by the $Z^{(2)}$ decay in the UED model [7]. Since the two subsequent decays $Z^{(2)} \to L^{(1)}L^{(1)}$ and $L^{(1)} \to \ell\gamma^{(1)}$ occur near the mass threshold, MASS I is to be called the "near threshold case". For comparison, we consider the mass parameters with sizable gap in MASS III, the "large mass gap

	m_D (GeV)	m_B (GeV)	m_a (GeV)	m_X (GeV)
MASS I	1250	600	0	550
MASS II	1000	440	0	300
MASS III	1000	350	0	200
MASS IV	600	250	m_Z	100

TABLE I: Test mass spectrum sets for mass measurements using kinematic cusp structure (m_Z is the Z boson mass).

case". The visibility of the cusp depends on the ratio $M_{aa}^{\rm cusp}/M_{aa}^{\rm max}$. As shown in Eq. (4), the distribution for $M_{aa} < M_{aa}^{\rm cusp}$ is linear, while that after $M_{aa}^{\rm cusp}$ is a concave curve with the maximum at $M_{aa}^{\rm max}/e$. The cusp becomes a sharper peak if $M_{aa}^{\rm cusp} \geq M_{aa}^{\rm max}/e$ (or equivalently $m_B > 0.44 m_D$). The parameters in MASS II are chosen to represent this boundary case of $m_B \approx 0.44 m_D$. The cusp structure is more pronounced for the near threshold case (MASS I), while it is less clear for the large mass gap case (MASS III).

(2) $m_a \neq 0$ case: If the SM particle a is massive (a Z boson or a top quark), we call it the "massive case", as for the parameter choice in MASS IV, that are motivated by the MSSM heavy Higgs boson decay associated with two SM Z bosons. In this case, the analytic form of $d\Gamma/dM_{aa}$ is given by three pieces (the explicit forms are not very illuminating and thus not given here). The maximum of M_{aa} is

$$M_{aa}^{\rm max} = 2m_a c_{\eta+\zeta}. \tag{5}$$

The positions of $M_{aa}^{\rm min}$ and $M_{aa}^{\rm cusp}$ are as follows, depending on the relations of the two rapidities η and ζ:

	$\eta < \zeta/2$	$\zeta/2 < \eta < \zeta$	$\zeta < \eta$
$M_{aa}^{\rm min}$	$2m_a$	$2m_a$	$2m_a c_{\eta-\zeta}$
$M_{aa}^{\rm cusp}$	$2m_a c_{\eta-\zeta}$	$2m_a c_\eta$	$2m_a c_\eta$

(6)

A few remarks are in order. First, the results of Eqs. (5) and (6) for $\eta < \zeta/2$ include the massless case, which corresponds to $\zeta \to \infty$. Second, for all three regions in Eq. (6), the M_{aa} distribution shows a sharp cusp, as illustrated by the MASS IV case in Fig. 2. Third, the case $\zeta < \eta$ has different $M_{aa}^{\rm min}$, rather than $2m_a$ as naively expected. It is due to the enhanced boost of the two fast-moving parent B's. This shift helps to resolve the ambiguity among the three regions. Still a two-fold ambiguity in the $\eta < \zeta/2$ and $\zeta/2 < \eta < \zeta$ regions remains since we do not know whether the measured $M_{aa}^{\rm cusp}$ is $2m_a c_{\eta-\zeta}$ or $2m_a c_\eta$.

We propose another independent observable to break this ambiguity, $(\Delta|p_T^a|)_{\rm max}$, which is the maximum of the difference between the magnitudes of the two transverse momenta of a_1 and a_2. We find the expression to be

$$\begin{aligned}(\Delta|p_T^a|)_{\rm max} &\equiv \max\left(|\vec{p}_T^{\,a_1}| - |\vec{p}_T^{\,a_2}|\right) \\ &= m_a\left[\sinh(\eta+\zeta) - \sinh|\eta-\zeta|\right],\end{aligned} \tag{7}$$

which is invariant under longitudinal boost. Note that the two-fold ambiguity happens when $\eta < \zeta$ leading to $(\Delta|p_T^a|)_{\rm max} = 2m_a \cosh\zeta \sinh\eta$. This $\sinh\eta$-dependence can provide independent information from $M_{aa}^{\rm cusp}$.

Cusp in Angular Distribution. Another useful observable is the distribution about $\cos\Theta$, where Θ is the angle of a visible particle, say a_1, in the c.m. frame of a_1 and a_2, with respect to their c.m. moving direction. We find the expression of $d\Gamma/d\cos\Theta$ in the D-rest frame for $m_a = 0$ to be remarkably simple:

$$\frac{d\Gamma}{d\cos\Theta} \propto \begin{cases} \sin^{-3}\Theta, & \text{if } |\cos\Theta| \leq \tanh\eta, \\ 0, & \text{otherwise.} \end{cases} \tag{8}$$

The distribution has a sharp end-point, another cusp, with the highest event rate at the boundary:

$$|\cos\Theta|_{\rm max} = \tanh\eta = \sqrt{1 - 4m_B^2/m_D^2}\ . \tag{9}$$

While this variable is unambiguous in the lab frame at a lepton collider, we cannot determine the longitudinal motion of the particle D in hadronic collisions. After convoluting with the parton distribution functions to convert it to the lab frame, $d\Gamma/d\cos\Theta$ in Eq. (8) is smeared. In Fig. 3, we compare the $\cos\Theta$ distribution in the rest frame of D (thin curves) with that in the lab frame at the LHC (thick curves) for the near threshold case (MASS I) and the large mass gap case (MASS III). We have assumed that D is produced by direct s-channel gg or $q\bar{q}$ annihilation so that the longitudinal momentum distribution of D is obtained from the parton distribution of the incident protons.

The convolution effects with the partons smear out the sharp $\cos\Theta$ cusp in the lab frame. For the near threshold case (MASS I), the two sharp rises at both ends get much less pronounced, although it is still possible to read the edge point off in the distribution. For the large mass gap case (MASS III), as the end point position approaches towards $\cos\Theta = \pm 1$, the sharpness of two cusps maintains better. It is interesting to note that the cusp in the M_{aa} distribution and that in the $\cos\Theta$ distribution provide complementary information for determining m_B. The invariant mass distribution yields a better resolution for the near threshold case, while the angular distribution provides better one for the large mass gap case.

To some extent, the $\cos\Theta$ distribution in the D-rest frame may be obtained even in hadron collisions. The smearing effects can be effectively modeled by the well-known parton distribution functions in the large x region. Or the direct resonant decay of D into SM particles allows to extract the velocity distribution of D, which can be used to recover $d\Gamma/d\cos\Theta$ in the D-rest frame.

Discussion. Until now, we have ignored the effects of the matrix elements regarding the spin correlations between the initial state and final state particles. We have confirmed that, for the four processes in Eq. (1), including the full matrix elements does not change the shape of the distributions. The deviations from the phase space

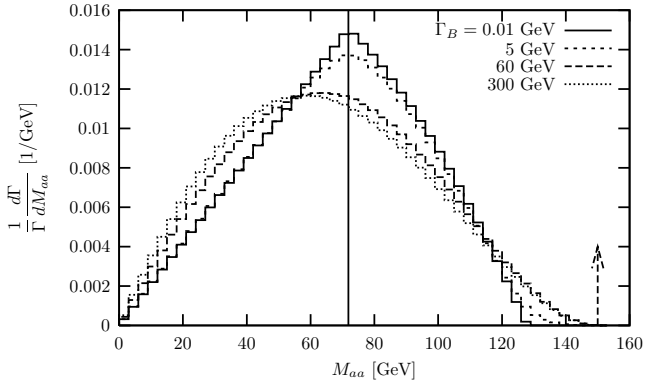

FIG. 4: The invariant mass distribution with the effect of the finite decay width for the MASS I case. We vary the total decay width Γ_B with $\Gamma_B = 0.01, 5, 60,$ and 300 GeV. The solid vertical line denotes the position of $M_{aa}^{\rm cusp}$.

predictions become appreciable when the fermions and vector bosons (like the $Z^{(2)}$ in UED) have chiral couplings for both $D \to BB$ and $B \to aX$ decays. Even in this extreme case, the cusped peak remains at the same location and its height is changed by about 2%.

However, non-vanishing decay widths of parent particles can alter the shape of the distributions. In Fig. 4, we show the M_{aa} distributions for different finite decay widths Γ_B with the MASS I spectrum. With $\Gamma_B \sim m_B/100$, such distortions do not have a big effect. With $\Gamma_B \sim m_B/10$, the finite decay width effect can change the cusp shape as well as the positions of $M_{aa}^{\rm cusp}$ and $M_{aa}^{\rm max}$. In the limit $\Gamma_B \sim m_B$, the momenta of the visible particles a_1 and a_2 span all of the allowed phase space given by m_D and m_X, regardless of m_B, and thus the maximum of M_{aa} approaches $m_D - 2m_X$, denoted by the vertical dashed arrow in Fig. 4. The end point measurement with the known m_D leads to the missing particle mass m_X, just like the direct neutrino mass determination in tritium decays. In the scenarios listed in Eq. (1), the intermediate particles ($\tilde{\chi}_2^0$, $\tilde{\ell}^\pm$, $L^{(1)}$ and t_-) typically have decay widths that are smaller than one percent of their masses. The cusp shape in the M_{aa} distribution remains intact.

Our cusp distributions of the signals are quite distinctive from the SM background kinematics. For instance, the leading SM backgrounds for $\ell^+\ell^- + \not{E}_T$ are mainly from $W^+W^-/ZZ \to \ell^+\ell^-\nu\bar{\nu}$, while those for $ZZ + \not{E}_T$ from ZZZ/W^+W^-Z, which should be well predicted in the SM. The optimal strategy to suppress the SM backgrounds is different case by case. We leave the detailed analyses to [9].

Conclusions. New techniques to measure the missing particle mass are proposed based on an "antler decay topology" ($D \to B + B \to aX + aX$), with a final state of two visible particles (a) and two missing particles (X) via intermediate particles (B). This antler decay has no combinatoric complications. We found cusp structures in the invariant mass distribution of two visible particles and an angular distribution. The cusp structure in the antler decay has large (in most cases largest) event rates unlike the end points. With its unique geometric feature, the cusp is easy to identify. Along with the end points of the distributions, the missing particle mass as well as the intermediate particle mass can be determined. A possible two-fold ambiguity can be resolved by another new observable, the difference between the magnitudes of transverse momenta of two observable SM particles. We believe that this technique will be invaluable for searches for new physics at the LHC.

Acknowledgments

This work is supported in part by the U.S. Department of Energy under grant No. DE-FG02-95ER40896. The work of JS was supported by the Korea Research Foundation Grant (KRF-2009-013-C00014).

[1] I. Hinchliffe, F. E. Paige, M. D. Shapiro, J. Soderqvist and W. Yao, Phys. Rev. D **55**, 5520 (1997); B. C. Allanach, C. G. Lester, M. A. Parker and B. R. Webber, JHEP **0009** (2000) 004 ; B. K. Gjelsten, D. J. Miller and P. Osland, JHEP **0412**, 003 (2004); M. Burns, K. T. Matchev and M. Park, JHEP **0905**, 094 (2009); K. T. Matchev, F. Moortgat, L. Pape and M. Park, arXiv:0906.2417.

[2] C. G. Lester and D. J. Summers, Phys. Lett. B **463**, 99 (1999) ; B. C. Allanach, C. G. Lester, M. A. Parker and B. R. Webber, JHEP **0009**, 004 (2000) ; A. Barr, C. Lester and P. Stephens, J. Phys. G **29**, 2343 (2003); C. Lester and A. Barr, JHEP **0712**, 102 (2007); P. Konar, K. Kong and K. T. Matchev, JHEP **0903**, 085 (2009).

[3] W. S. Cho, K. Choi, Y. G. Kim and C. B. Park, Phys. Rev. Lett. **100**, 171801 (2008) ; B. Gripaios, JHEP **0802**, 053 (2008) ; W. S. Cho, K. Choi, Y. G. Kim and C. B. Park, JHEP **0802**, 035 (2008); A. J. Barr, B. Gripaios and C. G. Lester, JHEP **0802**, 014 (2008).

[4] M. M. Nojiri, G. Polesello and D. R. Tovey, arXiv:hep-ph/0312317; K. Kawagoe, M. M. Nojiri and G. Polesello, Phys. Rev. D **71** (2005) 035008 ; H. C. Cheng, J. F. Gunion, Z. Han, G. Marandella and B. McElrath, JHEP **0712**, 076 (2007) ; H. C. Cheng, D. Engelhardt, J. F. Gunion, Z. Han and B. McElrath, Phys. Rev. Lett. **100**, 252001 (2008).

[5] A. Djouadi, Phys. Rept. **459**, 1 (2008).

[6] M. Baumgart, T. Hartman, C. Kilic and L. T. Wang, JHEP **0711**, 084 (2007).

[7] A. Datta, K. Kong and K. T. Matchev, Phys. Rev. D **72**, 096006 (2005) [Erratum-ibid. D **72**, 119901 (2005)]; H. C. Cheng, K. T. Matchev and M. Schmaltz, Phys. Rev. D **66**, 036005 (2002).

[8] A. Freitas, P. Schwaller and D. Wyler, arXiv:0906.1816.

[9] T. Han, I.W. Kim, J. Song, work in progress.